Available online at www.sciencedirect.com
ScienceDirect
Journal of the European Ceramic Society 27 (2007) 3691–3695
www.elsevier.com/locate/jeurceramsoc

In situ UV–vis and EXAFS studies of ZnO quantum-sized nanocrystals and Zn-HDS formations from sol–gel route

C.V. Santilli [a,*], S.H. Pulcinelli [a], M.S. Tokumoto [a,b], V. Briois [c]

[a] *Instituto de Química, UNESP, PO Box 355, 14800-900 Araraquara, SP, Brazil*
[b] *Departamento de Engenharia Química, UFSCar, Rodovia Washington Luiz, Km 235, PO Box 676, 13565-905 São Carlos, SP, Brazil*
[c] *Synchrotron SOLEIL, L'Orme des Merisiers, BP 48, 91 192 Gif-sur Yvette Cedex, France*

Available online 26 March 2007

Abstract

We have pointed out that, zinc-based particles obtained from zinc acetate sol–gel route is a mixture of quantum-sized ZnO nanoparticles, zinc acetate, and zinc hydroxide double salt (Zn-HDS). Aiming the knowledge of the mechanisms involved in the formation of ZnO and Zn-HDS phases, the thermohydrolysis of ethanolic zinc acetate solutions induced by lithium hydroxide ($[LiOH]/[Zn^{2+}] = 0.1$) or water ($[H_2O]/[Zn^{2+}] = 0.05$) addition was investigated at different isothermal temperatures (40, 50, 60 and 70 °C) by *in situ* measurements of turbidity, UV–vis absorption spectra and extended X-ray absorption fine structures (EXAFS). Only the growth of ZnO nanoparticles was observed in sol prepared with LiOH, while a two-step process was observed in that prepared with water addition, leading the fast growth of Zn-HDS and the formation of ZnO nanoparticles at advanced stage. A mechanism of dissolution/reprecipitation governed by the water/ethanol proportion is proposed to account for relative amount of ZnO.

Keywords: Sol–gel processing; Spectroscopy; X-ray methods; ZnO

1. Introduction

The 3.2 eV band gap of ZnO semiconductor results in an optical absorption edge at the ultraviolet (UV) end of the visible (vis) spectrum, and the carrier effective masses are sufficiently small such that band gap enlargement due to quantum confinement is observed for particle diameters less than about 8 nm.[1] This quantum size (QS) confinement becomes a very important effect because of its new and potential applications in the areas of UV laser, UV light-emitting diodes, field emission displays and spintronic[2,3] The excitonic peak and size-dependent blue shift in the UV–vis absorbance spectrum is currently used to identify the nanoparticles prepared by sol–gel route from zinc acetate-derivative precursor as single ZnO phase, while the by-products analysis on powdered samples and dip-coated or spin-coated films are usually neglected.[3–6]

Recently, we have pointed out that the powder extracted by solvent evaporation of sol–gel suspensions are constituted[7] of a mixture of nanometer-sized zinc oxide (ZnO), zinc acetate ($ZnAc_2{\cdot}2H_2O$), and acetate-derivative zinc hydroxide double salt (Zn-HDS). The sequence of formation of these phases is not clear, since Zn-HDS may be prepared either from reaction of zinc acetate salt with a basis or from dissolution/reprecipitation of ZnO nanoparticles in presence of zinc acetate salt.[8,9] More recently, we have shown that the thermohydrolysis of the ethanolic zinc acetate precursor solutions at 60 °C induced by addition of water[10] led to concomitant growth of ZnO and Zn-HDS at the early stage of hydrolysis and to ZnO dissolution during solvent evaporation.

In this paper, we analyse the different steps of ZnO nanoparticles and Zn-HDS formation by *in situ* monitoring of turbidity and UV–vis absorption spectra during the thermohydrolysis carried out between 40 and 70 °C of ethanolic zinc acetate precursor solutions promoted by addition of LiOH ($[LiOH]/[Zn^{2+}] = 0.1$) or water ($[H_2O]/[Zn^{2+}] = 0.05$). The zinc-based condensed phases formed after thermohydrolysis reactions carried out at different temperatures were identified and quantified by Zn K edge extended X-ray absorption fine structure (EXAFS) measurements done in the suspensions and dried powders.

2. Experimental

The preparation of ZnO sol has been fully described in Ref.[7] The $Zn_4O(CH_3COO)_6$ tetrameric precursor (noted

* Corresponding author at: Instituto de Química, UNESP, PO Box 355, 14800-900 Araraquara, SP, Brazil. Tel.: +55 16 33016645; fax: +55 16 33227932.
E-mail address: santilli@iq.unesp.br (C.V. Santilli).

0955-2219/$ – see front matter © 2007 Elsevier Ltd. All rights reserved.
doi:10.1016/j.jeurceramsoc.2007.02.019

above Zn_4OAc_6)[11] was first prepared by refluxing an absolute ethanol solution containing 0.1 mol L^{-1} zinc acetate dihydrate ($Zn(CH_3COO)_2{\cdot}2H_2O$ (noted above $ZnAc_2{\cdot}2H_2O$) (Synth)) for 3 h at 80 °C under magnetic stirring. Hydrolysis of the precursor solution was carried out at different isothermal temperature, between 40 and 70 °C, by adding LiOH ($[LiOH]/[Zn^{2+}] = 0.1$) or water ($[H_2O]/[Zn^{2+}] = 0.05$). Precipitates were separated from the solution after sedimentation by removal of the supernatant ethanolic solution and dried at 50 °C.

The time evolution of the turbidity during thermohydrolysis was measured *in situ* by using a Del Lab DLA 1000 nephelometer equipped with a thermostated cell and a tungsten polychromatic light. UV–vis absorption spectra were recorded in real time during thermohydrolysis by using a Varian Cary 50 UV–vis spectrophotometer equipped with a fiber optic coupler fitted to a thermostated polypropylene cell.[10] The average size of QS-ZnO particles was determined from the absorption spectra using the effective mass model derived by Brus.[1]

EXAFS data were measured at LURE (Orsay, France) using the DCI storage ring (1.85 GeV, 300 mA). The Zn K edge (9659 eV) EXAFS spectra of the liquid and powdered samples were recorded on the energy-dispersive D11 spectrometer equipped with a Si(1 1 1) curved monochromator using a Princeton CCD camera for detection. For the powder analysis, the final precipitates were ground and mixed with graphite in order to prepare pellets suitable for EXAFS characterization (i.e. a edge jumps in transmission mode of about $\Delta\mu x \approx 1$). The EXAFS treatment was performed by using the program developed by Michalowicz.[12] After atomic absorption removal based on cubic spline function and normalization, the $k^3\chi(k)$ weighted EXAFS signal was Fourier transformed to R (distance) space, using the 3.1–14.8 $Å^{-1}$ Kaiser apodization window with $\tau = 3$. As the samples are a mixture of two or three components (zinc precursor, QS-ZnO and/or Zn-HDS), our analysis was limited to the Fourier transforms (FT) and the experimental EXAFS spectra were fitted as linear combination of these components using the least square-fitting module available in the SIXPack software.[13]

3. Results and discussion

The evolution of the turbidity with the time of thermohydrolysis under different isothermal temperatures is shown in Fig. 1. As the turbidity is highly dependent on the volume fraction of particles in suspension, the increase of turbidity evidences the increasing number of particles with the reaction time. The comparison of the curves corresponding to samples prepared with LiOH (Fig. 1(a)) and H_2O (Fig. 1(b)) reveals different regimes: (i) *a first time period* in which the turbidity is essentially time invariant for LiOH-prepared sols. The same induction time period is verified whatever the thermohydrolysis temperature carried out in presence of LiOH, suggesting that the same kinetic processes occur under these conditions. This induction period is not observed for sols prepared by water addition; (ii) *a second time period* that is characterized by a pronounced increase of turbidity that grows faster as the reaction temperature increases. As a consequence the maximum turbidity value achieved by the sol prepared with LiOH at 40 °C is

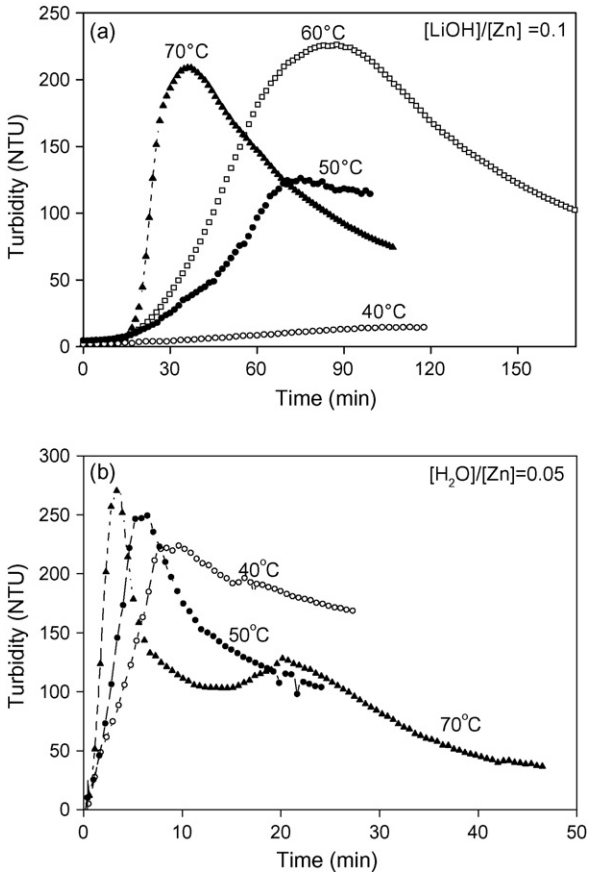

Fig. 1. Temporal evolution of the turbidity for thermohydrolysis carried out at the indicated isothermal temperature under: (a) LiOH and (b) water addition.

approximately 10 times lower than the maxima observed for sols prepared at higher temperature or with water; (iii) *a third time period* for which a fast decrease of turbidity occurs due to the settling of colloidal particles. This behaviour is observed when the samples have reached a high concentration of particles in suspension (turbidity > 200 FTU) favouring the aggregation and subsequent settling. Furthermore, it is important to note that this regime appears to be continuous in the samples prepared with LiOH at 60 and 70 °C, while it is stepped for sols prepared at 70 °C in presence of water. As it will be shown below, these different features revealed by the samples prepared with water and LiOH addition are not only due to larger volume fraction of particles formed in the former, but also due to different nature of zinc-based phase having larger particle sizes. Finally, we must anticipate here that the nature of zinc-based phase essentially depends on the catalyst added to initiate the hydrolysis–condensation reactions and not on the temperature. Based on this result, we can indifferently choose for the UV–vis and EXAFS data presented below those recorded at different temperatures for a given catalyst.

The raw UV–vis absorption spectra recorded during the thermohydrolysis of the zinc precursor solutions at 40 °C ($[LiOH]/[Zn^{2+}] = 0.1$) and 50 °C ($[H_2O]/[Zn^{2+}] = 0.05$) are shown in Fig. 2(a) and (b), respectively. During the *first time period* ($t < 10$ min), a well-resolved excitonic peak typical of QS-ZnO nanoparticle is observed below 330 nm in the sol pre-

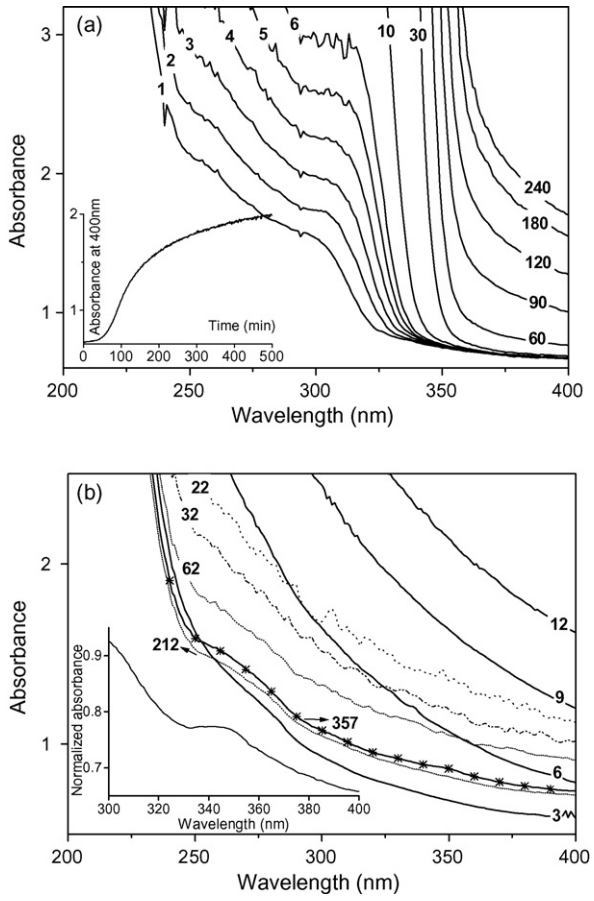

Fig. 2. Raw absorption spectra recorded during thermohydrolysis at (a) 40 °C under LiOH addition and (b) at 50 °C under water addition. The reaction time in minutes is indicated on the curves. The inset in (a) presents the time evolution of the absorbance measured at 400 nm. The inset in (b) is the absorption spectrum recorded at 357 min of hydrolysis normalized by the spectrum of the precursor solution.

pared with LiOH (Fig. 2(a)). As the reaction time increases from 1 to 6 min the onset of the excitonic peak progressively red shift from 324 to 337 nm evidencing a faint growth of average radius of QS-ZnO particles from 1.6 to 1.8 nm. Simultaneously to this red shift the intensity of the excitonic peak continuously increases indicating the formation of an increasing number of QS-ZnO particles. The spectrometer detector becomes saturated at $t > 7$ min hindering the monitoring of the QS-ZnO growth, in particular the observation of the excitonic peak and the accurate determination of the cut-off wavelength used for the determination of particle radius.[10] Nevertheless, in the period ranging from 10 to 60 min we can observe that the absorbance threshold is abrupt and shifts continuously up to 360 nm, suggesting that the QS-ZnO particles achieve an average radius of 2.6 nm. These behaviours suggest that during this period, both the number and the average size of ZnO particles increase. After 60 min, an increase of absorbance occurs in the whole visible range, that is probably related to light scattering caused by the formation of the large particles detected from the turbidity. This proposition is confirmed by time evolution of the absorbance measured at 400 nm (inset of Fig. 2(a)) that shows a perfect agreement with the temporal dependence of turbidity (Fig. 1(a)).

For the sol prepared at 50 °C with water (Fig. 2(b)), no clear evidence of the excitonic peak typical of QS-ZnO nanoparticles arises from the raw UV–vis spectrum during the whole time period of *in situ* monitoring. During the first 12 min, a fast increase of absorbance occurs in the whole spectrum, without the appearance of any characteristic feature. It is noteworthy that, this behaviour is totally in agreement with that observed during the *first and the second time period* revealed by turbidity measurements (Fig. 1(b)), showing that the scattering by the large particles dominates the UV–vis spectrum. After that, the opposite behaviour is observed, i.e. the whole absorbance decreases continuously with the reaction time until ≈210 min. Finally at advanced hydrolysis time ($t > 215$ min), a faint but significant and continuous increase of absorbance occurs on the whole UV–vis spectra suggesting the formation of a new family of particles. As a matter of fact, the spectrum recorded for the sol at the end of the kinetic normalized by that of precursor solution (inset of Fig. 2(b)) presents an excitonic peak around 340–350 nm that is typical of ZnO nanoparticles.

Further information about crystallochemical nature of Zn-based particles in solution and in the dried powder extracted at the end of synthesis was obtained from EXAFS measurements. Fig. 3 displays the Zn K edge EXAFS spectra recorded at the beginning and at the end of thermohydrolysis of sol prepared with addition of base (40 °C) or water (60 °C) and of the corresponding dried powders extracted at the end of each synthesis. For comparison purpose the spectra of solid nanocrystalline ZnO and of a nanocrystalline Zn-HDS reference are also displayed. It is first noteworthy that a common EXAFS spectrum is obtained for the powders extracted from sol prepared with LiOH or water addition, which is clearly in phase with the spectrum of the Zn-HDS reference. The EXAFS recorded at the beginning of both synthesis conditions displays as typical feature a relatively unstructured spectrum like the one of Zn_4OAc_6 precursor.[11] The

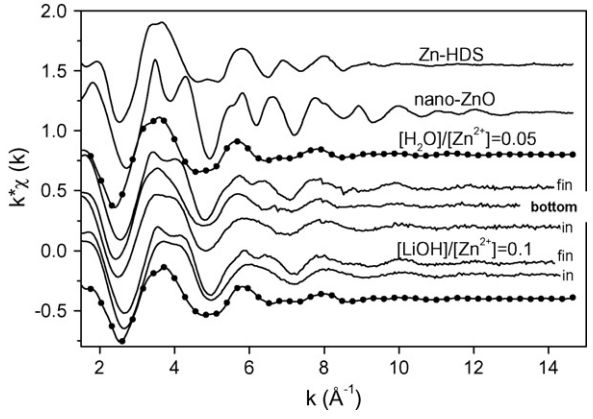

Fig. 3. EXAFS spectra recorded at the beginning (labeled 'in') and at the end (labeled 'fin') of thermohydrolysis carried out at 40 °C ($[LiOH]/[Zn^{2+}] = 0.1$) and at 60 °C ($[H_2O]/[Zn^{2+}] = 0.05$). The spectrum labeled bottom reported for the kinetic with water addition corresponds to the spectrum recorded at the bottom of the cell after settling of the particles formed during the first period of particles formation, i.e. at $t \approx 30$ min. The corresponding dried powder extracted at the end of each synthesis is displayed in dotted curves. The EXAFS spectra of powdered ZnO nanocrystalline, labeled nano-ZnO, and of a nanocrystalline Zn-HDS reference, are reported for comparison purpose at the top of the figure.

Table 1
Proportions of main compounds present in the sol and in the corresponding dried powder prepared with water and LiOH addition

Zn-Phase	Condition			
	Sol[a]	Powder[a]	Sol[b]	Powder[b]
ZnO	(29)		22	
Zn-HDS	24	49		43
Precursor	76 (71)	51	78	57

Values between parentheses correspond to proportion just before the settling of larger particles.
[a] $[H_2O]/[Zn^{2+}] = 0.05$.
[b] $[LiOH]/[Zn^{2+}] = 0.1$.

EXAFS oscillations observed in solution at the end of synthesis carried out with base or water are in phase with the characteristic oscillations measured on the spectrum of nano-sized ZnO reference. In particular, the splitting of the EXAFS oscillations in the 3–7 $Å^{-1}$ *k*-range, which is a characteristic fingerprint of ZnO, is well evidenced. The damping of EXAFS oscillations for samples compared to the nano-sized ZnO reference is due to the mixture between unreacted precursors and ZnO nanoparticles. The EXAFS data of sol formed by water addition recorded just after the settling of particles at the bottom of the cell is similar to the data reported for the dried powder, indicating that Zn-HDS particles were formed during the first time period of thermohydrolysis.

Table 1 summarises the proportion of Zn-based phases present in the sols and in the extracted dried powders prepared by LiOH or water addition estimated from linear combinations of EXAFS spectra of the main zinc species (nano-ZnO, Zn-HDS and unreacted precursors). A dispersion lower than 2% with respect to values gathered in Table 1 was found for thermohydrolysis carried out at different temperatures. This feature indicates that in the 40–70 °C range the temperature plays a minor role in the proportion and nature of Zn-based species formed by hydrolysis/condensation reactions. In agreement with the UV–vis absorption spectra the ZnO nanoparticles were undetected during the initial time of hydrolysis induced by water addition, for which the Zn-HDS component is the main product. Under this synthesis condition the QS-ZnO nanoparticles are only detected at advanced stage (see the inset of Fig. 2(b)) when stepped settling of large particles was observed. The fact that the amount of unreacted precursors is almost constant at the end of this two-stepped kinetic strongly suggests that the QS-ZnO particles result from a dissolution/reprecipitation process, involving the Zn-HDS particles formed at the early stage. Furthermore, the absence of detectable amount of Zn-HDS in the sol prepared with LiOH demonstrates that the control of the water amount is of paramount importance in sol–gel synthesis of QS-ZnO suspensions. Although the presence of QS-ZnO nanoparticles was well characterized at the advanced stage of synthesis carried out with water and LiOH addition, they are absent in the final dried powder precipitates. This evidence that the change of proportion water/ethanol due to the preferential evaporation of alcohol during drying displaces the equilibrium between dissolution/reprecipitation reactions favouring again the formation of Zn-HDS phase. Thus, to obtain QS-ZnO thin film from this sol–gel route, it is of paramount importance to extract the remnant water before the post-synthesis step. This can be done for instance by using molecular sieves or appropriated exchange resins.

4. Conclusions

The formation of Zn-HDS compound by the known sol–gel method used to prepare ZnO nanoparticles from zinc acetate in alcoholic solutions has been investigated as a function of thermohydrolysis temperature and addition of water or LiOH. The temperature of isothermal thermohydrolysis (between 40 and 70 °C) mainly affects the ZnO nanoparticle growth rate leading in all sols prepared with LiOH to a mixture of $22 \pm 2\%$ of ZnO nanoparticles and $78 \pm 2\%$ of unreacted precursors.

The paramount importance of water/ethanol proportion on chemical nature of Zn-based compounds present in the sol and in the dried powder was demonstrated by the comparative analysis of hydrolysis induced by LiOH and water addition. The later leads to fast growth of Zn-HDS and the formation of ZnO nanoparticles only occurs at the advanced stage. This two-stepped process evidences that in presence of small amount of water ($[H_2O]/[Zn] = 0.05$) the formation of ZnO nanoparticles is governed by dissolution/reprecipitation mechanism of Zn-HDS. The increase of water/alcohol ratio due to the preferential evaporation of alcohol during drying favours the dissolution of ZnO nanoparticles and the reprecipitation of Zn-HDS. As consequence Zn-HDS and precipitate zinc acetate precursor are the main components found in the final dried powders.

Acknowledgements

The authors thank the LURE staff for technical support during EXAFS experiments. This work has been financially supported by the FAPESP and CNPq (Brazil) and by a CAPES/COFECUB cooperation program between Brazil and France.

References

1. Brus, L. E., A simple model for the ionization potential electron affinity, and aqueous redox potentials of small semiconductor crystallites. *J. Phys. Chem.*, 1983, **79**, 5566–5571.
2. Tang, Z. K., Kawasaki, M., Ohtomo, A., Koinuma, H. and Segawa, Y., Self-assembled ZnO nano-crystals and exciton lasing at room temperature. *J. Cryst. Growth*, 2006, **287**, 169–179.
3. Schwartz, D. A., Norberg, N. S., Nguyen, Q. P., Parker, J. M. and Gamelin, D. R., Magnetic quantum dots: synthesis, spectroscopy and magnetism of Co^{2+} and Ni^{2+} doped ZnO nano crystals. *J. Am. Chem. Soc.*, 2003, **125**, 13205–13218.
4. Spanhel, L. and Anderson, M. A., Semiconductor clusters in sol–gel process: quantized agrregation, gelation and crystal growth in concentred ZnO colloids. *J. Am. Chem. Soc.*, 1991, **113**, 2826–2833.
5. Meulenkamp, E. A., Synthesis and growth of ZnO nanoparticles. *J. Phys. Chem. B*, 1998, **102**, 5566–5572.
6. Hu, Z., Oskam, G., Penn, R. L., Pesika, N. and Searson, P. C., The influence of anion on the coarsening kinetics of ZnO nanoparticles. *J. Phys. Chem. B*, 2003, **107**, 3124–3130.
7. Tokumoto, M. S., Pulcinelli, S. H., Santilli, C. V. and Briois, V., Catalysis and temperature dependence on the formation of ZnO nanoparticles and of

zinc acetate derivatives prepared by the sol–gel route. *J. Chem. Phys. B*, 2003, **107**, 568–574.
8. Liang, C., Shimizu, Y., Masuda, M., Sasaki, T. and Koshizaki, N., Preparation of layered zinc hydroxide/surfactant nanocomposite by pulsed-laser ablation in a liquid medium. *Chem. Mater.*, 2004, **16**, 963–965.
9. Morioka, H., Tagaya, H., Karasu, M., Kadokawa, J. and Chiba, K., Effects of zinc on the new preparation method of hydroxy double salts. *Inorg. Chem.*, 1999, **38**, 4211–4216.
10. Briois, V., Giorgetti, Ch., Dartyge, E., Baudelet, F., Tokumoto, M. S., Pulcinelli, S. H. and Santilli, C. V., *In situ* and simultaneous nanostructural and spectroscopic studies of ZnO nanoparticle and Zn-HDS formations from hydrolysis of ethanolic zinc acetate solutions induced by water. *J. Sol–Gel Sci. Techn.*, 2006, **39**, 25–36.
11. Tokumoto, M., Briois, V., Santilli, C. V. and Pulcinelli, S. H., Preparation of ZnO nanoparticles: structural study of the molecular precursor. *J. Sol–Gel Sci. Techn.*, 2003, **26**, 547–551.
12. Michalowicz, A., *EXAFS pour le Mac Logiciels pour la Chimie*. Société Française de Chimie, Paris, 1991, p. 102.
13. Webb, S., Sixpack, 2004, URL: http://www-ssrl.slac.standford.edu/swebb/sixpack.htm.